Rational Design Based on Bioactive Conformation Analysis of Pyrimidinylbenzoates as Acetohydroxyacid Synthase Inhibitors by Integrating Molecular Docking, CoMFA, CoMSIA, and DFT Calculations

Yan-Zhen He,[†] Yuan-Xiang Li,[†] Xiao-Lei Zhu,[†] Zhen Xi,*[,‡] Congwei Niu,[‡] Jian Wan,[†] Li Zhang,[†] and Guang-Fu Yang*[,†]

Key Laboratory of Pesticide & Chemical Biology, Ministry of Education, College of Chemistry, Central China Normal University, Wuhan, Hubei 430079, P.R. China, and State Key Laboratory of Elemento-Organic Chemistry, Nankai University, Tianjin 300071, P. R. China

Received June 27, 2007

Pyrimidinylthiobenzoates constitute an important kind of herbicides targeting acetohydroxyacid synthase (AHAS, EC 2.2.1.6), which catalyze the first common step in branched-chain amino acid biosynthesis. Due to the symmetry of 4,6-dimethoxypyrimidyl, there are two kinds of conformation of pyrimidinylthiobenzoates: one's phenyl is left-extending (named conformation-L); the other's phenyl is right-extending (named conformation-R). On the basis of the assumption that 3D quantitative structure−activity relationship (QSAR) models derived from the bioactive conformation should give the best result, a strategy of density-functional-theory-based 3D-QSAR was proposed to identify the bioactive conformation of pyrimidinylthiobenzoates by integrating the techniques of molecular docking, comparative molecular field analysis (CoMFA), comparative molecular similarity indices analysis (CoMSIA), and density functional theory calculation. The combination of three criteria of q^2, r^2, and r^2_{pred} obtained from CoMFA and CoMSIA analyses clearly indicated that conformation-R rather than conformation-L might be the bioactive conformation for pyrimidinylthiobenzoates. A further comparison between the two binding modes indicated that pyrimidinylthiobenzoates and sulfonylureas have very similar binding sites, such as Trp586, Arg380, and Pro192. However, Lys251 formed H bonds with sulfonylureas rather than pyrimidinylthiobenzoates. In addition, the orientation of phenyl groups of the two classes of compounds in the binding pocket were revealed to be opposite, which explained why the mutation of Pro192 displayed different sensitivity to sulfonylureas and pyrimidinylthiobenzoates. On the basis of the understanding of interactions between pyrimidinyl-thiobenzoates and AHAS, we designed and synthesized six 8-(4,6-dimethoxypyrimidin-2-yloxy)-4-methylphthalazin-1-one derivatives according to the 3D-QSAR models. The excellent correlation between the tested K_i values against wild-type *A. thaliana* acetohydroxyacid synthase and the predicted IC_{50} values demonstrated the high reliability of the established 3D-QSAR models. To our knowledge, this is the first report highlighting the binding mode of herbicidal pyrimidinylthiobenzoates, which consisted of the reported results of herbicide resistance.

INTRODUCTION

Acetohydroxyacid synthase (AHAS; also known as acetolactate synthase, EC 2.2.1.6, formerly EC 4.1.3.18), which is the first common enzyme in the biosynthetic pathway of the branched-chain amino acids, such as valine, leucine, and isoleucine, has been identified as an attractive target for several structurally diverse herbicides for many years.[1] AHAS-inhibiting herbicides, including sulfonylureas, imidazolinones, triazolopyrimidines, and pyrimidinylbenzoates, have been widely and rapidly adopted as they present a number of advantages such as low required dosages, low mammalian toxicity, broad-spectrum weed control, and flexible application timing in a wide variety of crops. However, AHAS resistance has been described in about 95 weed species worldwide,[2] and this number has shown to be increasing at an exponential rate. Therefore, it is a big challenge to develop novel herbicides against both resistant and wild AHAS.

In 2002, Duggleby and co-workers reported the first crystal structures of the free catalytic subunit of yeast AHAS.[3] Subsequently, five crystal structures of this catalytic subunit of yeast AHAS in complex with chlorsulfuron, sulfometuron methyl, metsulfuron methyl, and tribenuron methyl were determined by the same group at a resolutions of 2.8, 2.19, 2.34, 2.29, and 2.58 Å,[4,5] respectively. These crystal structures provided a solid experimental basis for understanding the detailed intermolecular interactions between a sulfonylurea herbicide and the residues involved in herbicide resistance. However, the molecular mechanism between other classes of herbicides with AHAS is still unclear. Therefore, a comparison of the binding difference of various AHAS inhibitors will be helpful for the molecular design of more potent inhibitors against both resistant and wild AHAS.

The objective of the present study was to understand the mechanism of intermolecular interaction between pyrimidinylbenzoates and AHAS. First, we presented a strategy for

* To whom correspondence should be addressed. E-mail: gfyang@mail.ccnu.edu.cn (G.F.Y.), zhenxi@nankai.edu.cn (Z.X.).
[†] Central China Normal University.
[‡] Nankai University.

10.1021/ci7002297 CCC: $37.00
Published on Web 09/22/2007

Table 1. Structure and Enzyme Inhibition Activity of Pyrimidinylbenzoates

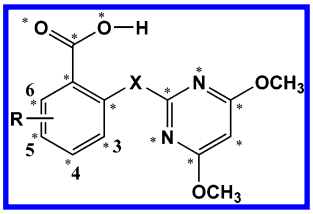

			pI_{50}				
				model-L[b]		model-R[c]	
no.[a]	R	X	obs.	CoMFA(7)[d]	CoMSIA(7)[e]	CoMFA(8)[d]	CoMSIA(8)[e]
				Training Set			
1	6-H	S	6.80	6.98	6.96	6.75	6.73
2	6-F	S	7.67	7.73	7.15	7.27	7.39
3	6-Cl	S	7.49	7.62	7.37	7.76	7.37
4	6-Br	S	7.40	7.43	7.21	7.38	7.18
5	6-I	S	6.99	7.42	7.23	7.33	7.20
6	6-CH_3	S	7.53	6.97	6.89	7.00	7.04
7	6-OC_2H_5	S	6.70	6.35	6.28	6.59	6.37
8	6-OC_3H_7	S	6.14	6.17	5.91	6.16	6.01
9	6-$OCH(CH_3)_2$	S	4.88	4.63	5.65	5.14	5.63
10	6-OC_6H_5	S	5.60	6.19	6.05	6.03	6.35
11	6-SCH_3	S	7.68	7.39	7.16	7.73	7.40
12	6-SC_2H_5	S	6.67	6.86	6.52	6.62	6.53
13	6-CF_3	S	6.02	6.04	6.51	5.97	6.00
14	6-NO_2	S	6.69	6.54	6.80	6.25	6.74
15	6-$COCH_3$	S	7.14	7.04	7.36	7.17	7.20
16*	6-COC_6H_5	S	5.19	5.22	5.87	5.29	5.27
17	6-H	O	6.64	6.41	6.05	6.38	6.12
18	6-F	O	7.30	7.31	7.49	7.42	7.57
19	6-Br	O	7.82	7.67	7.50	7.78	7.73
20	6-I	O	7.66	7.62	7.61	7.56	7.67
21	6-CH_3	O	6.89	7.48	7.25	7.19	7.28
22	6-C_2H_5	O	6.57	6.80	6.83	6.83	6.54
23	6-C_3H_7	O	5.89	6.10	6.25	6.14	5.90
24	6-OCH_3	O	7.36	7.20	7.02	7.52	7.27
25	6-OC_3H_7	O	6.24	5.95	6.15	6.06	6.15
26	6-$OCH(CH_3)_2$	O	5.73	5.85	6.30	5.69	5.74
27	6-OC_4H_9	O	6.21	6.12	6.26	6.14	5.98
28	6-$OCHF_2$	O	7.19	7.27	6.62	7.30	7.09
29	6-OC_6H_5	O	7.70	7.31	6.49	6.80	6.77
30	6-SCH_3	O	7.57	7.28	7.51	7.60	7.63
31	6-SC_3H_7	O	6.29	6.28	7.20	6.35	6.66
32	6-CF_3	O	6.96	6.65	6.99	6.70	6.59
33	6-NO_2	O	6.64	6.77	6.80	6.78	6.81
34	6-CO_2CH_3	O	5.68	5.72	5.70	5.55	5.55
35*	6-COC_6H_5	O	5.67	5.66	5.10	5.70	6.00
36*	6-C_6H_5	O	7.80	8.09	7.56	8.11	7.88
37	6-(1-pyrryl)	O	8.28	7.87	8.20	8.19	8.21
38	6-CH_3SO_2	O	5.87	6.20	5.16	5.90	5.76
39	6-NH_2	O	7.00	6.37	7.14	7.06	7.10
40	5-F	O	6.27	6.21	5.32	6.30	5.67
41	5-Br	O	4.50	4.88	4.80	4.58	5.14
42	5-I	O	5.05	4.87	4.53	4.80	4.77
43	5-CH_3	O	5.03	5.16	5.26	5.13	5.15
44	5-C_2H_5	O	4.59	4.48	5.00	4.61	4.34
45	5-OCH_3	O	4.60	4.98	5.65	4.53	4.24
46*	5-OC_6H_5	O	3.58	3.25	3.61	3.43	3.41
47	5-CN	O	3.71	3.76	3.68	3.81	3.83
48	5-NH_2	O	6.09	6.21	6.32	5.95	6.25
49	5-CCH	O	4.70	4.62	4.41	4.77	4.69
50	5-NO_2	O	3.90	3.95	4.48	4.13	4.19
51	5-OH	O	7.20	7.11	6.04	7.19	7.54
52	3-F	O	6.33	6.57	6.47	6.56	6.50
53	3-CH_3	O	5.39	5.71	6.31	5.51	5.85
54	5,6-$(Cl)_2$	O	6.03	6.24	6.55	6.06	6.55
				Test Set			
55	6-OCH_3	S	7.05	6.61	6.52	7.47	7.16
56	6-SC_3H_7	S	5.72	6.73	6.54	6.46	6.40
57	6-Cl	O	7.62	7.76	7.63	7.89	7.81

Table 1 (Continued)

			pI_{50}				
				model-L[b]		model-R[c]	
no.[a]	R	X	obs.	CoMFA(7)[d]	CoMSIA(7)[e]	CoMFA(8)[d]	CoMSIA(8)[e]
58	6-OC_2H_5	O	7.05	6.21	6.55	6.48	6.42
59	6-SC_2H_5	O	7.11	6.67	7.50	6.63	6.85
60	6-$COCH_3$	O	6.84	6.80	7.42	7.23	6.48
61	5-Cl	O	5.35	4.85	4.78	4.70	5.24
62	5-SCH_3	O	4.32	3.40	3.69	4.19	4.16

[a] The compounds failed in FlexX-Pharm docking are labelled with an asterisk. [b] The conformations used to construct model L were based on the DFT-optimized results using the conformation 30-L as a template. [c] The conformations used to construct model R were based on the DFT-optimized results using the conformation 30-R as a template. [d] Calculated using the CoMFA model. [e] Calculated using the CoMSIA model with the steric, electrostatic, and hydrophobic fields.

deriving the bioactive conformation of pyrimidinylbenzoates by integrating the techniques of comparative molecular field analysis (CoMFA)[6] and comparative molecular similarity indices analysis (CoMSIA),[7] conformation analysis, and density functional theory (DFT) calculation. Further, using the program of AutoDock, the derived bioactive conformation was docked into the binding pocket of AHAS. The resulting binding mode of pyrimidinylbenzoates was compared with that of sulfonylureas revealed in the crystal structures of AHAS complex. Then, some new compounds were designed and synthesized according to the established 3D quantitative structure−activity relationship (QSAR) models. To our knowledge, this is the first report on the interaction between pyrimidinylbenzoates and AHAS, which might provide a new starting point for the design of new inhibitors against both wild and resistant AHAS.

MATERIALS AND METHODS

Data Sets. All dimethoxypyrimidinyl(thio)salicylic acids and their *in vitro* biological activity (pI_{50} values) were taken from the literature,[8] from which a set of eight molecules chosen at random was used as the test set, while the remaining 54 compounds were treated as a training set. The general structure of all of the compounds is shown in Table 1. The synthetic chemistry, characterization data, and AHAS assay of newly designed compounds **63**−**68** are available in the Supporting Information.

Molecular Docking. The FlexX-Pharm program[9] interfaced with Sybyl 7.0[10] was used to perform the docking procedure. The 3D coordinates of the AHAS binding site were taken from the X-ray crystal structure of the yeast AHAS in complex with a commercial sulfonylurea herbicide chlorimuron ethyl (PDB code: 1N0H).[4]

It has been established that the Trp574 mutation of *Arabidopsis thaliana* AHAS, corresponding to Trp586 of yeast AHAS, resulted in resistance to all classes of AHAS inhibitors,[11−13] which revealed that Trp574 was the overlapped binding site for AHAS-inhibiting herbicides. The crystal structure of yeast AHAS in complex with sulfonylureas indicated that the pyrimidinyl formed $\pi-\pi$ stacking interactions with residue Trp586. Therefore, we proposed that the dimethoxypyrimidinyl interacted with residue Trp586 *via* $\pi-\pi$ stacking, as the pyrimidinyl had proven previously to be the common structure of herbicidal sulfonylureas and pyrimidinylbenzoates and was shown to be an electron-transfer site.[14] Next, amino acids within 6.5 Å of the cocrystallized ligand were defined as the binding pocket, and three FlexX-Pharm constraints were defined (see the Supporting Information): A $\pi-\pi$ stacking interaction between the indolyl group of Trp586 and dimethoxypyrimidinyl was defined. NH1 and NH2 of Arg380 were set as hydrogen-bond donors. In order to prevent the phenyl group of pyrimidinylbenzoates from stacking onto the indolyl plane of Trp586, a spatial constraint was defined delineating the essential presence of a nitrogen atom within the area 1.5 Å from the center of the pyrimidinyl ring of chlorimuron ethyl.

Molecular Modeling and Alignment. All molecular modeling and calculations studies were performed using the Sybyl 7.0[10] and Gaussian 03 programs[20] running on an SGI Origin 300 server. The 3D structures of all compounds were built from the Sybyl fragment library and energy-minimized using a conjugate gradient minimization algorithm with Gasteiger−Hückel charges. Moreover, they were docked into the binding site of yeast AHAS. The ligand and amino acids within 10 Å of chlorimuron ethyl in the obtained docking complex with the highest total score were subsequently optimized using an Amber7 FF99 force field. Next, the ligands were extracted and optimized using the DFT method with the B3LYP functional. The 3-21G basis set was employed for the iodine atom, while the 6-31G(d, p) basis set[17] was used for all other kinds of atoms. Vibrational frequencies were computed at the same level to characterize stationary points. Net atomic charges were derived from Merz−Singh−Kollman[18,19] methods that produce charges suitable for the electrostatic potential at selected points. Compound **30** was used as a template and all other compounds were aligned on the basis of the common structure marked with an asterisk as shown in Table 1.

CoMFA and CoMSIA Descriptors. CoMFA steric and electrostatic interaction fields were calculated at each lattice intersection on a regularly spaced grid of 2.0 Å. The grid pattern was generated automatically by the Sybyl/CoMFA routine and extended 4.0 Å units in the *X*, *Y*, and *Z* directions beyond the dimensions of each molecule. An sp^3 carbon atom with a van der Waals radius of 1.52 Å and a +1.0 charge was used as the probe to generate the steric field energies and electrostatic fields with a distance-dependent dielectric at each lattice point. Values of the steric and electrostatic fields were truncated to 30.0 kcal mol^{-1}. The CoMFA steric and electrostatic fields generated were scaled by the CoMFA-STD method in Sybyl. The electrostatic fields were ignored at the lattice points with maximal steric interactions.

CoMSIA similarity indices descriptors were calculated with the same lattice box as was used for the CoMFA

Table 2. Summary of the Effects of Optimization Methods and Charge Types on the 3D-QSAR Results

	Tripos/GAST_HUCK				AM1/AM1			
	model-L		model-R		model-L		model-R	
	CoMFA(1)	CoMSIA(1)[a]	CoMFA(2)	CoMSIA(2)	CoMFA(3)	CoMSIA(3)	CoMFA(4)	CoMSIA(4)
q^2	0.694	0.387	0.730	0.513	0.629	0.082	0.707	0.213
S_{press}	0.682	0.945	0.641	0.890	0.759	1.111	0.675	1.049
r^2	0.943	0.806	0.968	0.924	0.975	0.331	0.980	0.620
s	0.296	0.531	0.220	0.351	0.197	0.949	0.178	0.729
comp.	7	5	7	10	8	1	8	3
F	107.790	39.990	200.170	52.568	219.575	25.699	271.140	27.162
				Contribution				
Ste	0.718	0.248	0.675	0.225	0.645	0.115	0.584	0.214
Ele	0.282	0.322	0.325	0.283	0.355	0.533	0.416	0.488
Hydro		0.430		0.492		0.352		0.298
r_{pred}^2	0.6874	0.9226	0.8344	0.8717	0.9296	0.301	0.8582	0.9623
	PM3/PM3				DFT/ESP			
	model-L		model-R		model-L		model-R	
	CoMFA(5)	CoMSIA(5)[a]	CoMFA(6)	CoMSIA(6)	CoMFA(7)	CoMSIA(7)	CoMFA(8)	CoMSIA(8)
q^2	0.643	0.140	0.688	0.069	0.711	0.555	0.788	0.720
S_{press}	0.737	1.076	0.681	1.130	0.656	0.797	0.562	0.651
r^2	0.957	0.384	0.960	0.572	0.947	0.810	0.960	0.921
s	0.256	0.910	0.245	0.766	0.281	0.521	0.244	0.347
comp.	7	1	6	2	6	4	6	7
F	145.675	32.396	187.048	34.029	140.188	52.269	188.254	76.218
				Contribution				
Ste	0.560	0.124	0.531	0.153	0.474	0.203	0.502	0.244
Ele	0.440	0.547	0.469	0.543	0.526	0.569	0.498	0.503
Hydro		0.329		0.303		0.228		0.253
r_{pred}^2	0.6963	0.5471	0.8978	0.7807	0.7876	0.8252	0.8357	0.8794

[a] CoMSIA using the steric, electrostatic, and hydrophobic fields.

calculations. The similarity index $A_{F,k}$ for a molecule j with atoms i at the grid point q is determined as follows:

$$A_{F,k}^{q}(j) = \sum_i \omega_{probe,k}\omega_{ik}\, e^{-\alpha r_{iq}^2}$$

where ω_{ik} is the actual value of the physicochemical property k (steric, electrostatic, hydrophobic, hydrogen-bond donor, and hydrogen-bond acceptor), which was evaluated using the probe atom. A Gaussian-type distance dependence was used between the grid point q and each atom i of the molecule. The default value of 0.3 was used as the attenuation factor α.

A partial least-squares (PLS) approach,[21−23] which is an extension of multiple regression analysis, was used to derive the 3D-QSAR models, in which the CoMFA and CoMSIA descriptors were used as independent variables and pI_{50} values were used as dependent variables. Prior to the PLS analysis, CoMFA and CoMSIA columns with a variance smaller than 2.0 kcal mol^{-1} were filtered by using column filtering to improve the signal-to-noise ratio. The cross-validation with the leave-one-out option was carried out to obtain the optimal number of components, followed by a non-cross-validated analysis with the same column filtering set. The q^2 (cross-validated r^2), S_{press} (cross-validated standard error of prediction), r^2 (non-cross-validated r^2), and F values and standard error of estimate (s) values were computed according to the definitions in Sybyl 7.0 and are shown in Table 2.

The q^2 (cross-validated r^2) term is sensitive to the orientation of aligned molecules on the computer terminal and may vary with the orientation by as much as 0.5 q^2 units,[24] so we used the all-orientation search method,[25] which could find the optimum orientation of the molecular alignment aggregates within the grid yielding the highest q^2, to get more consistent results in CoMFA studies after alignment.

RESULTS AND DISCUSSION

Deriving the Bioactive Conformation by a DFT/3D-QSAR Strategy. In the case of using the plane of dimethoxypyrimidinyl as a reference, the docking results indicated that the phenyl of 62 ligands adopted two different orientations, with some being left-extending, while others were right-extending. In order to determine which one (left-extending conformation and right-extending conformation) is the true orientation, a DFT/3D-QSAR strategy was proposed for the analysis of the bioactive conformation of dimethoxypyrimidinylbenzoates, which is based on the assumption that the 3D-QSAR models based on the bioactive conformation should give the best result.

First, the conformation of compound **30** in the docking complex after optimizing with the Amber7 FF99 force field was extracted and used as a template (named 30-L) to construct another 61 molecules (named the 30-L series). Meanwhile, the phenyl of conformation 30-L was turned to the opposite direction (named 30-R), which was used as the other template to construct another 61 molecules (named the 30-R series). These two series of conformations were then optimized using DFT methods. The initial and DFT-optimized conformations of 30-L and 30-R are shown in Figure 1.

CoMFA and CoMSIA. As the real bioactive conformation of the title compounds was unknown, two different 3D-

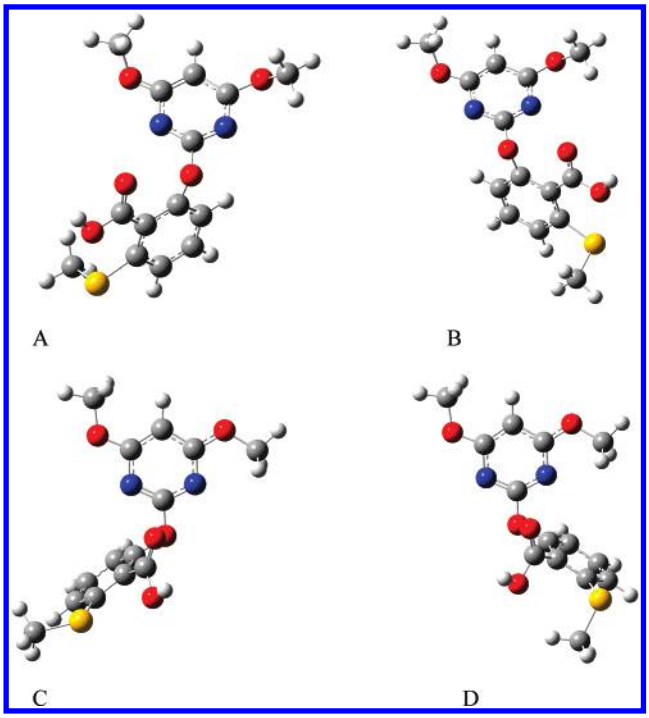

Figure 1. The conformations of compound **30**. (A) The conformation after optimizing the docked complex using Amber FF99 force field. (B) The conformation after the phenyl in conformation A was turned to the opposite position. (C) DFT-optimized conformation-based conformation A (30-L). (D) DFT-optimized conformation-based conformation B (30-R).

QSAR models (named model-L and model-R) were built on the basis of 61 DFT-optimized conformations of the 30-L series and 30-R series, respectively. The alignment rule of common substructure consisting of atoms labelled with asterisks in compound **30** (as shown in Table 1) was used, and the results of CoMFA and CoMSIA studies are summarized in Table 2. The combination of steric, electrostatic, and hydrophobic fields always gave the highest q^2 value in CoMSIA analyses, so only the CoMSIA results using steric, electrostatic, and hydrophobic fields were listed. In addition, the effects of different types of charge (Gasteiger−Hückel charge, AM1 charge, PM3 charge, and DFT electron spin polarization, ESP, charge) and conformation-optimizing methods (Tripos force field, AM1 method, PM3 method, and DFT method) on the 3D-QSAR results were also listed in Table 2.

From Table 2, we can conclude that not only the conformation-optimizing methods but also the types of atomic charge play an important role in building satisfactory 3D-QSAR models. Compared with that of model-L, the CoMFA and CoMSIA analyses of model-R always gave higher q^2 value. In addition, the DFT-optimized conformation and ESP charges derived from DFT calculation based on model-R gave the best COMFA and CoMSIA results with the cross-validated q^2 value of 0.788 for six components and 0.720 for seven components, respectively. The non-cross-validated PLS analyses were repeated with the optimum number of components, as determined by the cross-validated analyses, to give r^2 values of 0.960 and 0.921 for CoMFA and CoMSIA analyses, respectively. These correlation coefficients suggest that both the CoMFA and CoMSIA models based on the conformation of the 30-R series are reliable and accurate. In the best CoMFA and CoMSIA models, the contribution of the electrostatic fields is almost equal (49.8% in CoMFA, 50.3% in CoMSIA). In addition, the CoMSIA model indicated that the hydrophobic field was also an important factor for the inhibitory activity, which accounted for 25.3% of the actual variance in activity. Besides, we also examined the effects different types of charge based on DFT-optimized conformation had on the 3D-QSAR results (see the Supporting Information), which also indicated that ESP charge derived from DFT calculation gives the best results.

The observed and calculated activity values for the training set molecules are given in Table 1. The plots of the predicted versus the actual activity values for the training set are shown in Figure 2. As seen in Table 1 and Figure 2, the trained CoMFA and CoMSIA models could reproduce the experimental data very well for all the compounds included in the training set. However, the real test for the model predictability was to predict the activity of compounds that were not included in the training set. Therefore, we used a test set consisting of eight randomly selected compounds (list in Table 1) to challenge the predictability of the obtained models. The results were also shown in Table 1 and Figure 2, which indicated that the activity of all the compounds in the test set was estimated well. As shown in Table 2, both the CoMFA(8) and CoMSIA(8) models based on the conformation of the 30-R series gave the highest r_{pred}^2 values of 0.8357 and 0.8794, respectively. Further, the combination of three criterions of q^2, r^2, and r^2_{pred} clearly indicated that conformation 30-R might be the most proximate one to the bioactive conformation. It has been depicted that these obtained 3D-QSAR models can be used as predictive tools in the future rational design of AHAS inhibitors with the desirable higher activity.

Structure-Based Interpretation of 3D-QSAR Models. The greatest advantage of CoMFA and CoMSIA is that the field effect on the target property can be viewed as 3D coefficient contour plots. The coefficient contour plots are helpful to identify important regions where any change in the steric, electrostatic and hydrophobic fields may affect the biological activity, and in addition may also help to identify the possible interaction sites. In Figures 3−5, the isocontour diagrams of the field contributions ("stdev*coeff") of different properties obtained from the CoMFA and CoMSIA analyses are illustrated together with exemplary ligands.

The steric field contour maps of CoMFA and CoMSIA are plotted in Figure 3. The green displays positions where a bulky group in a dimethoxypyrimidinyl(thio)salicylic acid is introduced, which would be favorable for higher inhibition of AHAS. In contrast, yellow indicates positions where a decrease in the bulk of the dimethoxypyrimidinyl(thio)-salicylic acid is favored. As shown in Figure 3, the CoMFA and CoMSIA steric contours plots all obviously indicated that a yellow region, which was occupied by the residue of Pro192, is located around the 5′ substituent of the aryl ring. This means that the bulky substituents at the 5′ position will conflict with residue Pro192 and decrease the inhibitory activity. In addition, the CoMFA steric contours plots showed a green region near the 6′ substituent, while the CoMSIA steric contours plots indicated the existence of a near green region and an outer yellow region around 6′ substituents. These facts revealed that the steric effect of 6′ substituents might have an optimal value. For example, the activity of

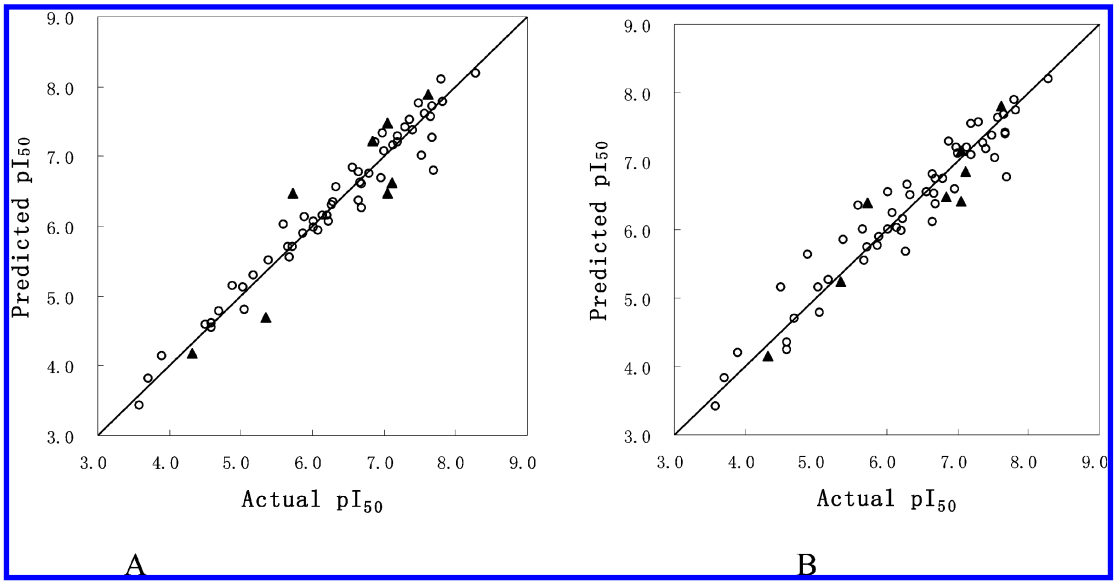

Figure 2. Plots of predicted pI_{50} versus experimental pI_{50}. (A) CoMFA(8) results based on model III. (B) CoMSIA(8) results based on model III. "○" and "▲" represent the training set and test set, respectively.

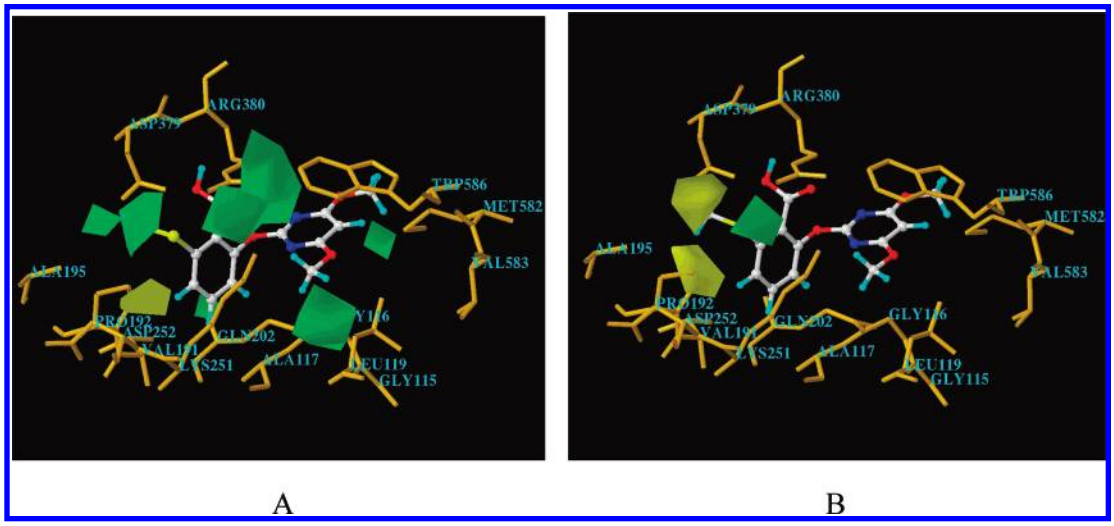

Figure 3. Steric contour plots from the CoMFA(8) (A) and CoMSIA(8) (B) analyses mapped on to the binding site of yeast AHAS. Sterically favored areas are represented by green contours (80% for CoMFA, 0.025 level for CoMSIA). Sterically disfavored areas are represented by yellow contours (20% for CoMFA, −0.070 level for CoMSIA).

compound **11** (6-SCH_3) was shown to be much higher than that of compound **1** (6-H), while compound **12** (6-SC_2H_5) exhibited lower activity than compound **11**. Moving the same substituent from the 6′ position to the 5′ position (compounds **18** and **40**, **19** and **41**) decreased the potency. In addition, there is another green region in the CoMFA contour maps, which was occupied by the hydrogen bond between the carboxyl group and the indolyl of Trp586, which indicates that the carboxyl group must adopt a favorable conformation to form a H bond with the indolyl of Trp586. DFT optimization showed that the torsion angle between the carboxyl plane and the benzene ring is influenced by the substituents; the 6′ substituent made the carboxyl group rotate into the green region.

The electrostatic contour plots are shown in Figure 4. The blue contour defines a region where an increase in the positive charge will result in an increase in the activity, whereas the red contour defines a region of space where increasing electron density is favorable. When the CoMSIA contour maps are taken as an example, a red contour in the vicinity of the 6′ subsitituents indicates that electronegative groups at this position could help to increase the activity, such as compounds **2**, **3**, **4**, **18**, **19**, **28**, and **37**. A blue contour around 5′ substituents, corresponding to the area of negatively charged residue of Asp252, showed that electropositive groups at this position would be favorable to increase the inhibitory activity.

The hydrophobic fields of the CoMSIA model are shown in Figure 5. Gray and yellow contours indicated the areas where hydrophilic and hydrophobic properties were preferred, respectively. A large yellow and three small gray regions appeared around the 6′ substituent, which indicated that a group with an optimal hydrophobicity at the 6′ position resulted in a positive effect on the potency. In addition, a very distinct hydrophilic site can also be observed near the 5′ position, which suggested that an interaction between the Asp252 and a hydrophilic group at the 5′ substituent might improve the inhibitory activity. For example, compound **51** having a 5-OH substituent displayed the highest pI_{50} value among the 5′ substituted compounds.

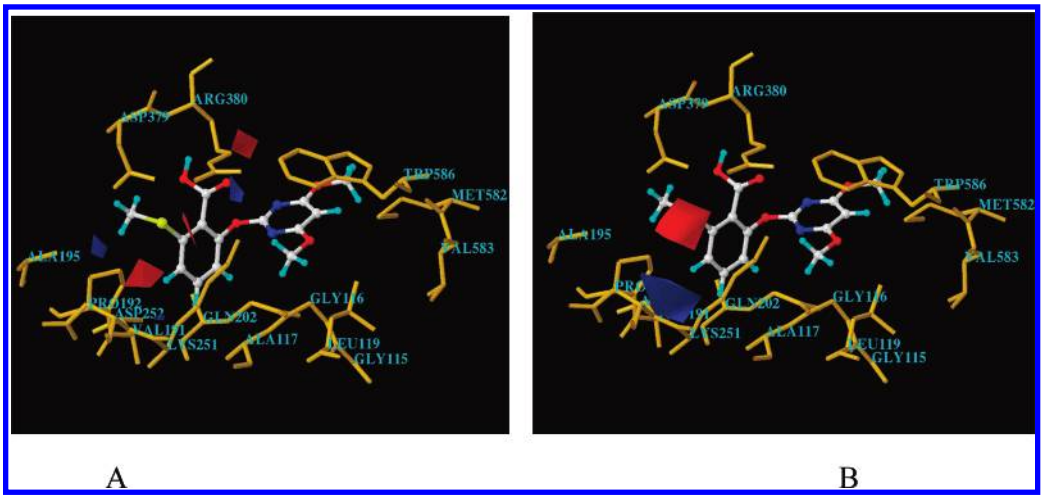

Figure 4. Electrostatic contour plots from the CoMFA(8) (A) and CoMSIA(8) (B) analyses mapped on to the binding site of yeast AHAS. Positive-charge-favored areas are represented by blue contours (80% for CoMFA, 0.110 level for CoMSIA). Negative-charge-favored areas are represented by red contours (20% for CoMFA, −0.140 level for CoMSIA).

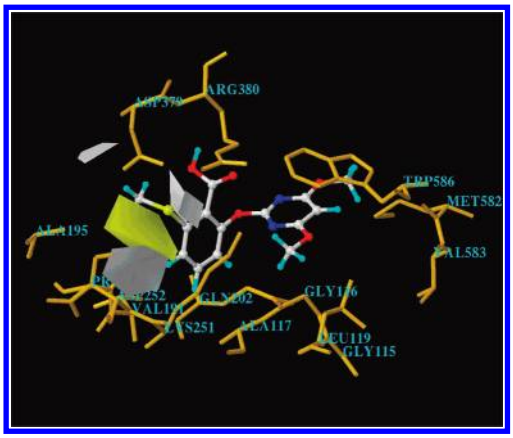

Figure 5. Hydrophobic contour plots from the CoMSIA(8) analyses mapped onto the binding site of yeast AHAS. Yellow regions indicate areas where hydrophobic groups increase activity (0.040 level), and gray regions indicate areas where hydrophilic groups will increase activity (−0.030 level).

Comparison of the 3D-QSAR Models with the X-ray Crystal Structure of AHAS in Complex with Sulfonylureas. It has been proved that site mutation displayed different sensitivity to structurally diverse inhibitors, so it is very interesting to compare the binding mode of pyrimidinylthiobenzoates and sulfonylureas with AHAS, which will provide important information for the further design of more potent inhibitors against both resistant and wild AHAS. Then, we docked the highest active compound, **37**, into the binding pocket of AHAS using the AutoDock 3.05 program. The conformation 37-R of compound **37** was kept rigid during the docking process. The Lamarckian genetic algorithm was used to explore the energy landscape. A docking box of 62 × 82 × 58 points with a grid spacing of 0.375 Å centered on the coordinates 23.394, 127.338, 45.332, which is approximately the center of the binding site, was used in the calculations. The binding mode of chlorimuron ethyl revealed by X-ray diffraction analysis was shown in Figure 6A, which shows that four amino acid residues, Trp586, Arg380, Lys251, and Pro192, were involved in the chlorimuron ethyl−AHAS interactions. The pyrimidinyl of chlorimuron ethyl formed a strong $\pi-\pi$ stacking interaction with the indolyl group of Trp586 and the oxygen and nitrogen atoms of pyrimidinyl; the oxygen atom of the bridge carboxyl formed four hydrogen bonds with Arg380; moreover, two additional hydrogen bonds were also observed between the bridged atoms as acceptors and Lys251 as a donor. In addition, the phenyl of chlorimuron ethyl interacted with Pro192 *via* hydrophobic interaction. Figure 6B showed

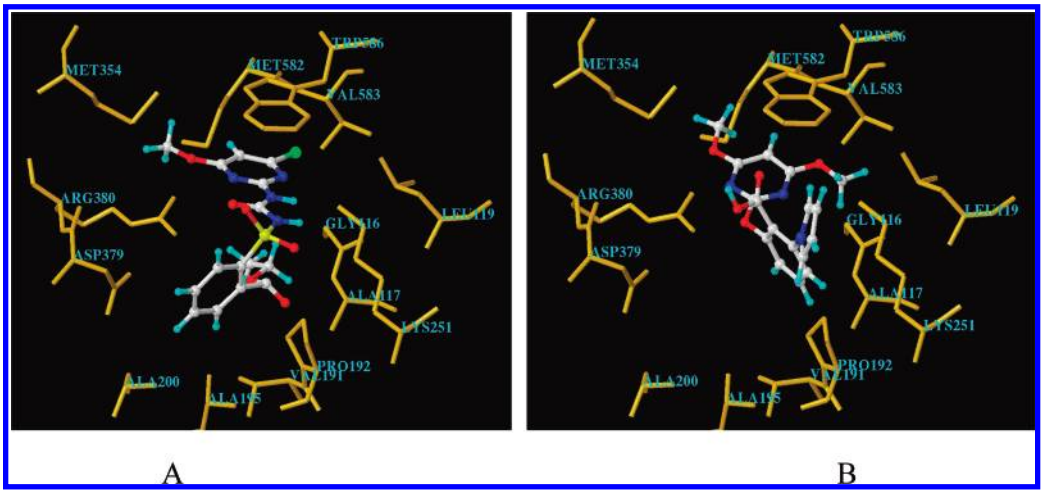

Figure 6. The conformation of chlorimuron ethyl (A) and compound **37** (B) in the binding site from the crystal structure and docking results, respectively.

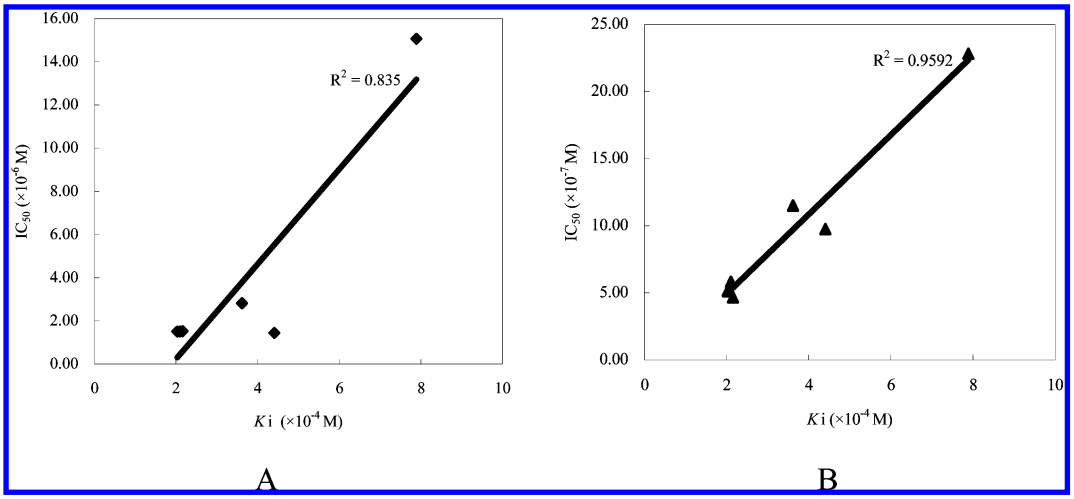

Figure 7. The plots of the predicted IC_{50} values versus the actual K_i values of compounds **63**−**68** (A, CoMFA model; B, CoMSIA model).

Scheme 1. Design of the 8-(4,6-Dimethoxypyrimidin-2-yloxy)-4-methylphthalazin-1-one Derivatives

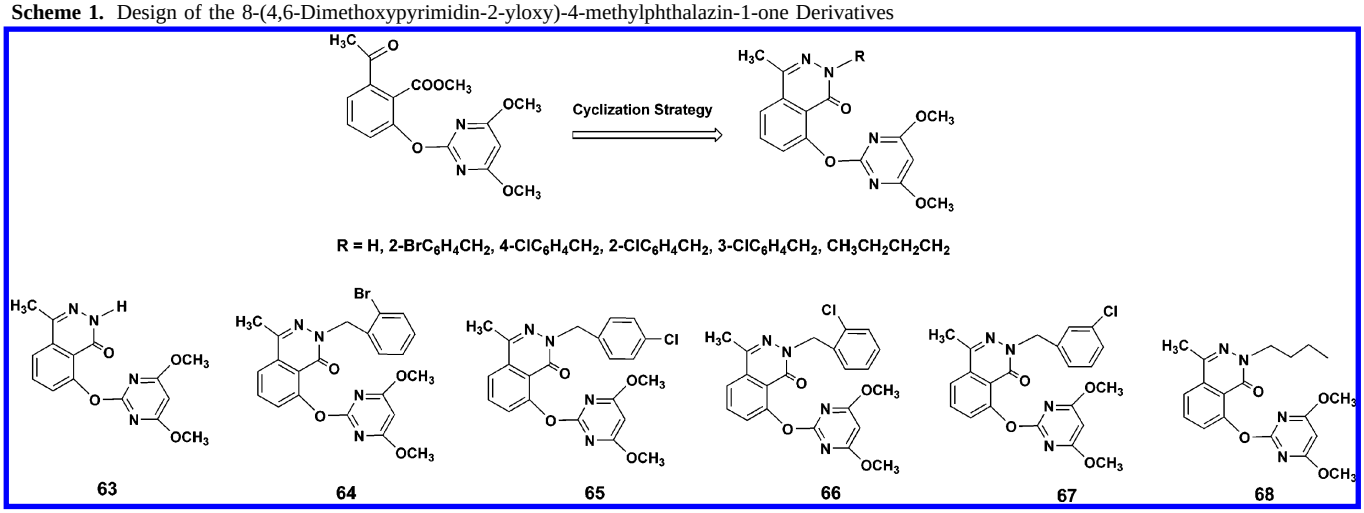

that the binding mode of compound **37** with AHAS was very similar to that of chlorimuron ethyl, which is consistent with the reported results of herbicidal-resistant studies. For example, Trp586 interacted with the dimethoxypyrimidinyl of compound **37** *via* $\pi-\pi$ stacking, and Pro192 hydrophobically interacted with the phenyl of the compounds. In addition, four similar H bonds between Arg380 and compound **37** were also observed; also, an additional H bond between Arg380 and the oxygen atom of the carboxyl group was also observed. On the contrary, Lys251 did not interact with compound **37**, which was different as compared to chlorimuron ethyl. Most importantly, the phenyl groups of chlorimuron ethyl and compound **37** interacted hydrophobically with Pro192, but their orientations in the binding pocket were significantly different. This difference could be the reason why the mutation of Pro192 displayed a different sensitivity to sulfonylureas and pyrimidinylthiobenzoates. For example, it was reported that P192H in *Lactuca serriola* AHAS caused much higher resistance to sulfonylureas than pyrimidinylthiobenzoates.[26]

Rational Design Based on 3D-QSAR and Docking Models. An analysis of CoMFA and CoMSIA contour maps revealed that steric-favored and hydrophobic-favored regions exist both around the 6 position and the 6 substituents extended outside the binding pocket. In addition, both the oxygen atoms of the carboxyl group at 1 position played a role as a H bond acceptor. On the basis of these observations, we developed an idea that if we have the ortho substituents at the 1 and 6 positions to form a ring and keep some H-bond acceptors at the ring, the resulting structure might display good AHAS-inhibiting activity. Then, we designed and synthesized some 8-(4,6-dimethoxypyrimidin-2-yloxy)-4-methylphthalazin-1-one derivatives, **63**−**68** as shown in Scheme 1 (the synthetic chemistry and characterization data can be found in the Supporting Information), and determined their K_i values against wild type *A. thaliana* acetohydroxyacid synthase. The predicted IC_{50} values and the tested K_i values of compounds **63**−**68** are listed in Table 3, and the plots of the predicted IC_{50} values versus the actual K_i values of compounds **63**−**68** are shown in Figure 7. As seen in Table 3 and Figure 7, the CoMFA(8) and CoMSIA(8) models based on conformation-R series reproduce the experimental data very well for compounds **63**−**68** with correlation coefficients of $r^2 = 0.835$ and $r^2 = 0.9592$, respectively. However, the CoMFA(7) and CoMSIA(7) models based on conformation-L reproduce the experimental data for compounds **63**−**68** with

Table 3. The Predicted IC_{50} Values and the Tested K_i Values of Compounds **63**−**68**

compounds	**63**	**64**	**65**	**66**	**67**	**68**
tested K_i value ($\times 10^{-4}$ M)	7.89	3.62	2.03	2.10	2.16	4.41
predicted IC_{50} by CoMFA model ($\times 10^{-6}$ M)	15.07	2.82	1.50	1.50	1.52	1.45
predicted IC_{50} by CoMSIA model ($\times 10^{-7}$ M)	22.80	11.51	5.14	5.82	4.68	9.75

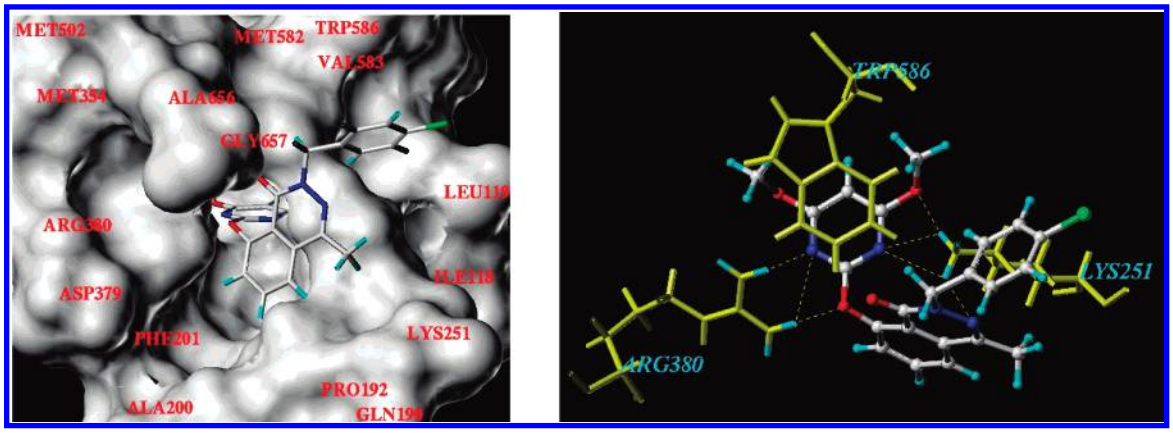

Figure 8. Molecular docking and interaction force of compound **65** with AHAS.

very bad correlation coefficients of $r^2 = 0.402$ and $r^2 = 0.0573$ (data and plots can be found in the Supporting Information), respectively, which further indicated that conformation-R might be the most proximate one to the bioactive conformation. In addition, molecular docking was conducted for the most active compound, **65**, as demonstrated in Figure 8, from which we can find that the dimethoxypyrimidinyl group of compound **65** adopted a similar binding mode as that of compound **37**, while compound **65** extended its *p*-chlorophenyl group outside the binding pocket. Interaction analysis indicated that Trp586 interacted with the dimethoxypyrimidinyl of compound **65** *via* $\pi-\pi$ stacking, and three similar H bonds between Arg380 and compound **65** were formed. In particular, four H bonds between Lys251 and compound **65** can also be observed. It should be noted that Lys251 did not interact with compound **37**, which means that compound **65** might be active against the resistant weeds for compound **37**.

CONCLUSION

Understanding the intermolecular interactions of a series of O-(4,6-dimethoxypyrimidin-2-yl)salicylic acids and their thio analogs with AHAS was achieved by integrating the techniques of molecular docking, CoMFA, CoMSIA, and density functional theory calculation. The best 3D-QSAR models were obtained on the basis of DFT-optimized conformation-R at the DFT/B3LYP level. A set of 3D contour plots drawn on the basis of the 3D-QSAR models revealed some useful clues to understand the structure−activity relationships of pyrimidinylthiobenzoates. Some binding sites revealed by the present study were a result of the reported findings of herbicidal resistance studies. Further, a comparison between two binding modes of pyrimidinylthiobenzoates and sulfonylureas indicated that these two classes of herbicides had very similar binding sites, such as Trp586, Arg380, and Pro192. However, Lys251 formed H bonds with sulfonylureas rather than pyrimidinylthiobenzoates. In addition, the orientation of phenyl groups of these classes of compounds in the binding pocket was shown to be opposite of each other. To our knowledge, this is the first report delineating the binding mode of herbicidal pyrimidinylthiobenzoates. On the basis of the understanding of interactions between pyrimidinylthiobenzoates and AHAS, we designed and synthesized six 8-(4,6-dimethoxypyrimidin-2-yloxy)-4-methylphthalazin-1-one derivatives according to the 3D-QSAR models. The excellent correlation between the tested K_i values against wild type *A. thaliana* acetohydroxyacid synthase and the predicted IC_{50} values demonstrated the high reliability of the established 3D-QSAR models.

ACKNOWLEDGMENT

The present work was supported by National "973" Project (2003CB114400), national NSFC grants (Nos. 20572030, 20432010, and 20528201), the Cultivation Fund of the Key Scientific and Technical Innovation Project, Ministry of Education of China (No.705039), and Program for Excellent Research Group of Hubei Province (No. 2004ABC002).

Supporting Information Available: The constraints defined in FlexX-Pharm; docking results by FlexX-Pharm; superimpositions of title compounds of three models; and the synthetic chemistry, characterization data, and AHAS assay of newly designed compounds **63**−**68**. This material is available free of charge via the Internet at http://pubs.acs.org.

REFERENCES AND NOTES

(1) Duggleby, R. G.; Pang, S. S. Acetohydroxyacid synthase. *J. Biochem. Mol. Biol.* **2000**, *33*, 1−36.
(2) Heap, I. International survey of herbicide resistant weeds. http://www.weedscience.com (accessed July 4, 2006).
(3) Pang, S. S.; Duggleby, R. G.; Guddat, L. W. Crystal structure of yeast acetohydroxyacid synthase: a target for herbicidal inhibitors. *J. Mol. Biol.* **2002**, *317*, 249−262.
(4) Pang, S. S.; Guddat, L. W.; Duggleby, R. G. Molecular basis of sulfonylurea herbicide inhibition of acetohydroxyacid synthase. *J. Biol. Chem.* **2003**, *278*, 7639−7644.
(5) McCourt, J. A.; Pang, S. S.; Guddat, L. W.; Duggleby, R. G. Elucidating the specificity of binding of sulfonylurea herbicides to acetohydroxyacid synthase. *Biochemistry* **2005**, *44*, 2330−2338.
(6) Cramer, R. D., III; Paterson, D. E.; Bunce, J. D. Comparative molecular field analysis (CoMFA). 1. Effect of shape on binding of steroids to carrier proteins. *J. Am. Chem. Soc.* **1988**, *110*, 5959−5967.
(7) Klebe, G.; Abraham, U.; Mietzner, T. Molecular similarity indices in a comparative analysis (CoMSIA) of drug molecules to correlate and predict their biological activity. *J. Med. Chem.* **1994**, *37*, 4130−4146.
(8) Nezu, Y.; Wada, N.; Yoshida, F.; Miyazawa, T.; Shimizu, T.; Fujita, T. Dimethoxypyrimidines as novel herbicides. Part 4. Quantitative structure-activity relationships of dimethoxy-pyrimidinyl(thio)salicylic acids. *Pestic. Sci.* **1998**, *52*, 343−353.
(9) Hindle, S.; Rarey, M.; Buning, C.; Lengauer, T. Flexible docking under pharmacophore type constraints. *J. Comput.-Aided Mol. Des.* **2002**, *16*, 129−149.
(10) *Sybyl*, version 7.0; Tripos Inc.: St. Louis, MO, 2004.
(11) Tranel, P. J.; Wright, T. R. Resistance of weeds to ALS-inhibiting herbicides: what have we learned? *Weed Sci.* **2002**, *50*, 700−712.
(12) Bernasconi, P.; Woodworth, A. R.; Rosen, B. A.; Subramanian, M. V.; Siehl, D. L. A naturally occurring point mutation confers broad range tolerance to herbicides that target acetolactate synthase. *J. Biol. Chem.* **1995**, *270*, 17381−17385.
(13) Tranel, P. J.; Wright, T. R; Heap, I. M. ALS mutations from herbicide-resistant weeds. http://www.weedscience.com (accessed April 24, 2006).

(14) Yang, G. F.; Liu, H. Y.; Lu, R. J.; Yang, H. Z. Design, synthesis and biological activity of novel herbicides targeted ALS (VI)−The Electronic structure of herbicidal pyrimidinyl(thio)ether compounds and the molecular design of novel herbicides. *Gaodeng Xuexiao Huaxue Xuebao* **1998**, *19*, 222−227.
(15) Becke, A. D. A new mixing of Hartree−Fock and local density-functional theories. *J. Chem. Phys.* **1993**, *98*, 1372−1377.
(16) Becke, A. D. Density-functional thermochemistry. III. The role of exact exchange. *J. Chem. Phys.* **1993**, *98*, 5648−5652.
(17) Petersson, G. A.; Bennett, A.; Tensfeldt, T. G.; Al-Laham, M. A.; Shirley, W. A.; Mantzaris, J. A complete basis set model chemistry. I. The total energies of closed-shell atoms and hydrides of the first-row elements. *J. Chem. Phys.* **1988**, *89*, 2193−2218.
(18) Besler, B. H.; Merz, K. M., Jr.; Kollman, P. A. Atomic charges derived from semiempirical Methods. *J. Comput. Chem.* **1990**, *11*, 431−439.
(19) Singh, U. C.; Kollman, P. A. An approach to computing electrostatic charges for molecules. *J. Comput. Chem.* **1984**, *5*, 129−145.
(20) Frisch, M. J.; Trucks, G. W.; Schlegel, H. B.; Scuseria, G. E.; Robb, M. A.; Cheeseman, J. R.; Montgomery, J. A.; Vreven, T., Jr.; Kudin, K. N.; Burant, J. C.; Millam, J. M.; Iyengar, S. S.; Tomasi, J.; Barone, V.; Mennucci, B.; Cossi, M.; Scalmani, G.; Rega, N.; Petersson, G. A.; Nakatsuji, H.; Hada, M.; Ehara, M.; Toyota, K.; Fukuda, R.; Hasegawa, J.; Ishida, M.; Nakajima, T.; Honda, Y.; Kitao, O.; Nakai, H.; Klene, M.; Li, X.; Knox, J. E.; Hratchian, H. P.; Cross, J. B.; Adamo, C.; Jaramillo, J.; Gomperts, R.; Stratmann, R. E.; Yazyev, O.; Austin, A. J.; Cammi, R.; Pomelli, C.; Ochterski, J. W.; Ayala, P. Y.; Morokuma, K. G.; Voth, A.; Salvador, P.; Dannenberg, J. J.; Zakrzewski, V. G.; Dapprich, S.; Daniels, A. D.; Strain, M. C.; Farkas, O.; Malick, D. K.; Rabuck, A. D.; Raghavachari, K.; Foresman, J. B.; Ortiz, J. V.; Cui, Q.; Baboul, A. G.; Clifford, S.; Cioslowski, J.; Stefanov, B. B.; Liu, G.; Liashenko, A.; Piskorz, P.; Komaromi, I.; Martin, R. L.; Fox, D. J.; Keith, T.; Al-Laham, M. A.; Peng, C. Y.; Nanayakkara, A.; Challacombe, M.; Gill, P. M. W.; Johnson, B.; Chen, W.; Wong, M. W.; Gonzalez, C.; Pople, J. A. *Gaussian 03*, Revision C.02; Gaussian, Inc.: Wallingford, CT, 2004.
(21) Wold, S.; Rhue, A.; Wold, H.; Dunn, W. J., III. The collinearity problem in linear regression. The partial least squares approach to generalized inverses. *SIAM J. Sci. Stat. Comput.* **1984**, *5*, 735−743.
(22) Wold, S.; Albano, C.; Dunn, W. J., III.; Edlund, U.; Esbensen, K.; Geladi, P.; Hellberg, S.; Johanson, E.; Lindberg, W.; Sjostrom, M. Multivariate data analysis in chemistry. *NATO Adv. Study Inst. Ser., Ser. C* **1984**, *138*, 17−95.
(23) Clark, M.; Cramer, R. D., III. The probability of chance correlation using partial least squares (PLS). *Quant. Struct.-Act. Relat.* **1993**, *12*, 137−145.
(24) Cho, S. J.; Tropsha, A. Cross-validated R^2-guided region selection for comparative molecular field analysis: a simple method to achieve consistent results. *J. Med. Chem.* **1995**, *38*, 1060−1066.
(25) Wang, R. X.; Gao, Y.; Liu, L.; Lai, L. H. All-orientation search and all-placement search in comparative molecular field analysis. *J. Mol. Model.* **1998**, *4*, 1−7.
(26) Eberlein, C. V. Altered acetolactate synthase activity in ALS-inhibitor resistant prickly lettuce (*Lactuca serriola*). *Weed Sci.* **1997**, *45*, 212−217.

CI7002297